Eur. Phys. J. B **5**, 237–243 (1998)

THE EUROPEAN PHYSICAL JOURNAL B

A new simulation method for the determination of forces in polymer/colloid systems

J. Jimenez and R. Rajagopalan[a]

Department of Chemical Engineering, University of Florida, Gainesville, Florida 32611-6005, USA

Received: 15 May 1998 / Revised: 11 June 1998 / Accepted: 12 June 1998

Abstract. We introduce a new simulation method, which we call the *contact-distribution method*, for the determination of the Helmholtz potential for polymer/colloid systems from lattice Monte-Carlo simulations. This method allows one to obtain forces between finite or semi-infinite objects of any arbitrary shape and dimensions in the presence of polymer chains in solution or physisorbed or chemisorbed at interfaces. We illustrate the application of the method using two examples: (i) the interaction between the tip of an atomic force microscope (AFM) and a single, end-grafted polymer chain and (ii) the interaction between an AFM tip and a polymer brush. Numerical results for the first two cases illustrate how the method can be used to confirm and extend scaling laws for forces and Helmholtz potentials, to examine the effects of the shapes and sizes of the objects and to examine conformational transitions in the polymer chains.

PACS. 36.20.-r Macromolecules and polymer molecules – 36.20.Ey Conformation (statistics and dynamics) – 02.70.Lq Monte-Carlo and statistical methods

1 Introduction

Interactions between polymers and colloidal surfaces play a central role in a large number of chemical, biological and materials sciences and processes. The understanding of these forces and the methods to determine them experimentally and theoretically are essential for tailoring polymer additives and polymer-induced forces in an increasing number of applications of both scientific and industrial relevance. In this context, the importance of computer simulations as a tool to test theories, to interpret experimental measurements or to just provide a better understanding of a given problem is evident.

In this work we introduce a new method based on Monte-Carlo (MC) simulations for determining the forces in polymer/colloid systems. The method is general enough to allow examination of systems with chemisorbed (*i.e.*, grafted) or physisorbed polymer chains on surfaces of arbitrary shape and dimensions and is computationally very efficient. We have already used this method, in a preliminary communication, to examine the interaction between an AFM tip and a polymer mushroom [1]. The objective of the present paper is to present the details of the simulation method and to illustrate its application through an extension of our previous work on polymer mushrooms and new results for polymer brushes.

[a] e-mail: `raj@eng.ufl.edu`

The paper is organized as follows: in Section 2 we review briefly two methods available in the literature, one for determining forces between a bare surface and a polymer coated one and the other for determining free energy differences from MC simulations in any general system (*i.e.*, not necessarily containing polymers). We draw from these two methods to formulate the new simulation technique for obtaining the force and Helmholtz potential. Section 3 presents the details of the new technique, which we call the *contact-distribution method*, and Section 4 illustrates its application to two different problems, namely, the interaction between an AFM tip and a single end-grafted polymer chain and the interaction of the AFM tip and a polymer brush. We also comment briefly on the application of the method to study the interaction of two particles in a polymer solution.

2 Free energy differences from Monte-Carlo data

Obtaining the Helmholtz potentials (and, therefore, the forces) from Monte-Carlo simulations is not straightforward. As a prelude to the method we propose in the next section, here we review briefly two techniques that are related to the focus of this paper. One of these is the *repulsive-wall technique* of Dickman [2–4], which he has

used to determine the force due to compression of a polymer brush by a bare surface ("wall"). The other is a technique introduced by Bennet [5] for estimating free-energy differences between two systems (not necessarily containing polymers) from simulations. It will be seen in Section 3 how these two techniques relate to the method proposed in this paper.

2.1 Repulsive-wall technique

For introducing the repulsive-wall technique, we consider a three-dimensional lattice with two planar surfaces separated from each other by a distance $z = H$. We take the surface located at $z = 0$ to be coated with polymer chains and the surface at $z = H$ to be a bare surface. The force of interaction between the two surfaces arising from the presence of the polymer chains is simply the change in free energy as the bare surface is moved from $z = H$ to $z = H - 1$. This change in the Helmholtz potential can be written as

$$\beta\Delta\mathcal{F} = \int_0^1 \frac{\partial \ln Q}{\partial \lambda} d\lambda, \tag{1}$$

where Q is the partition function of the system and λ is a parameter defined as $\lambda = e^{-\beta V}$, with V being a fictitious potential applied to the lattice plane immediately next to the bare wall (*i.e.*, $z = H - 1$). Note that $\lambda = 1$ corresponds to $V = 0$, that is, the bare surface is at $z = H$; in contrast, $\lambda = 0$ (*i.e.*, $V = \infty$) implies that the bare surface is at $z = H - 1$ (since the excluded-volume criterion prevents the polymer segments from the adjoining surface from occupying $z = H - 1$).

Equation (1) can be evaluated from the average number of contacts made by the polymer segments with the wall (*i.e.*, the average number of segments occupying the layer at $z = H - 1$) for a number of values of V between 0 and ∞. Note that the derivative in equation (1) can be written in terms of the number of polymer segments N_c in layer $H - 1$ as follows:

$$\begin{aligned}\frac{\partial \ln Q}{\partial \lambda} &= \frac{\sum N_c e^{-\beta\mathcal{U}} \lambda^{N_c - 1}}{\sum e^{-\beta\mathcal{U}} \lambda^{N_c}} \\ &= \frac{1}{\lambda}\langle N_c \rangle,\end{aligned} \tag{2}$$

where the configurational energy $\mathcal{U}$ does not include the contribution $N_c V$, which is written separately as shown. Equation (1) then becomes

$$\beta\Delta\mathcal{F} = \int_0^1 \frac{\langle N_c \rangle}{\lambda} d\lambda. \tag{3}$$

The above integral is evaluated by performing simulations for different values of V, and hence, for different values of λ. (Dickman [2] suggests that at least six values of λ be used.) One calculates $\langle N_c \rangle$ from each simulation and obtains the value of $\langle N_c \rangle / \lambda$ at $\lambda = 0$ (*i.e.*, $V = \infty$) by extrapolation. Equation (3) is then evaluated by numerical integration. This method is computationally demanding and is not very accurate if $\langle N_c \rangle / \lambda$ is not a smooth function that can be extrapolated easily to $\lambda = 0$.

2.2 Acceptance-ratio method

The other technique that is of interest here, developed by Bennet [5], is called the *acceptance-ratio method* and was introduced as an efficient way to estimate free energy differences from Monte-Carlo data in any kind of system. It considers two systems, denoted as 0 and 1, with configurational energies $\mathcal{U}_0$ and $\mathcal{U}_1$ obtained from respective pair-potentials u_0 and u_1. The ratio of the canonical partition functions of these systems, which defines the difference in Helmholtz energy $\beta\Delta\mathcal{F} = \ln(Q_0/Q_1)$, can be written as

$$\frac{Q_0}{Q_1} = \frac{Q_0}{Q_1} \frac{\int d\mathbf{r}^N w(\mathbf{r}^N) e^{-\beta(\mathcal{U}_0 + \mathcal{U}_1)}}{\int d\mathbf{r}^N w(\mathbf{r}^N) e^{-\beta(\mathcal{U}_0 + \mathcal{U}_1)}} = \frac{\left\langle w(\mathbf{r}^N) e^{-\beta\mathcal{U}_0} \right\rangle_1}{\left\langle w(\mathbf{r}^N) e^{-\beta\mathcal{U}_1} \right\rangle_0}, \tag{4}$$

where $w(\mathbf{r}^N)$ is a weight function for the configuration specified by $\mathbf{r}^N$, the positions of the N particles in the system. The optimum choice for $w(\mathbf{r}^N)$ is obtained by minimizing the statistical error in $\beta\Delta\mathcal{F}$ with respect to $w(\mathbf{r}^N)$ [5,6]. Such a procedure leads to

$$\frac{Q_0}{Q_1} = \frac{\left\langle \{1 + e^{-\beta(\mathcal{U}_0 - \mathcal{U}_1 + C)}\}^{-1} \right\rangle_1}{\left\langle \{1 + e^{-\beta(\mathcal{U}_1 - \mathcal{U}_0 - C)}\}^{-1} \right\rangle_0} e^{\beta C}, \tag{5}$$

where C is a constant. Rewriting equation (5) in terms of the Fermi-Dirac function

$$g(x) = \frac{1}{1 + e^{\beta x}},$$

one obtains

$$\frac{Q_0}{Q_1} = \frac{\langle g(\mathcal{U}_0 - \mathcal{U}_1 + C) \rangle_1}{\langle g(\mathcal{U}_1 - \mathcal{U}_0 - C) \rangle_0} e^{\beta C}. \tag{6}$$

Bennet [5] has shown that the optimal choice of C, denoted henceforth as C^*, corresponds to

$$e^{\beta C^*} = \frac{Q_0}{Q_1} \frac{n_1}{n_0}, \tag{7}$$

where n_0 and n_1 are the numbers of statistically independent samples taken from systems 0 and 1, respectively. Substituting for (Q_0/Q_1) in equation (6) and taking $C = C^*$, one gets

$$\sum_{i=1}^{n_1} g(\mathcal{U}_{0,i}^{(1)} - \mathcal{U}_{1,i}^{(1)} + C^*) = \sum_{i=1}^{n_0} g(\mathcal{U}_{1,i}^{(0)} - \mathcal{U}_{0,i}^{(0)} - C^*), \tag{8}$$

where $\mathcal{U}_{1,i}^{(j)}$ is the energy obtained from the ith sample of system j using the pair-potential u_1 and, similarly, $\mathcal{U}_{0,i}^{(j)}$ is the energy calculated with the pair-potential u_0.

(Note that one needs to run simulations of both systems and that the Boltzmann sampling in each system is based on its own configurational energy. For example, $\mathcal{U}_{1,i}^{(0)}$ is the configurational energy calculated using the pair-potential u_1 for a sample which is chosen with a probability proportional to exp $(-\beta\mathcal{U}_0)$ from system 0.) Once C^* is obtained from equation (8), it can be substituted into equation (7) for (Q_0/Q_1) so that $\Delta\mathcal{F}$ can be obtained from

$$\ln\left(\frac{Q_0}{Q_1}\right) = \beta\Delta\mathcal{F} = \beta C^* - \ln\frac{n_1}{n_0}\,. \tag{9}$$

In Section 3 below we use these two methods to develop a new technique to obtain forces from Monte-Carlo simulations. The new technique is computationally efficient and requires only two simulations to obtain the force in contrast to Dickman's method.

3 The new technique: contact-distribution method

Similar to the situation in the above section, we begin with two systems labelled 0 and 1. System 0 is a lattice of sides $L_x \times L_y$ and height L_z that contains a certain number of polymer chains and a "hard-body" (*i.e.*, an object that occupies a certain number of lattice sites and interacts with the polymer chains only through excluded-volume effects). System 1 is identical in every respect but has a repulsive potential V (> 0) at the moving boundary of the "hard-body"[1]. All other interaction energies (*e.g.*, polymer segment/segment interaction energy) remain the same in both systems. With this definition, the difference between the configurational energies of the two systems is given by

$$\mathcal{U}_1 - \mathcal{U}_0 = N_c V, \tag{10}$$

where N_c is the number of contacts (*i.e.*, number of segments of the polymer chains in the layer next to the moving boundary of the object). Substituting equation (10) in equation (8) and assuming that the numbers of samples from systems 0 and 1 are the same (*i.e.*, $n_0 = n_1 = n$), one gets

$$\sum_{(System\ 1)} g(C^* - N_c^{(1)}V) = \sum_{(System\ 0)} g(N_c^{(0)}V - C^*) \tag{11}$$

where $N_c^{(i)}$ is the number of contacts in system i.

Now, let $P_k^{(1)}$ be the probability of the polymer chains having k contacts with the hard body in system 1 (*i.e.*, in the system with repulsive potential V at the boundary) and $P_k^{(0)}$ the corresponding probability in system 0 (*i.e.*, in the system with no repulsive potential). One can then rewrite equation (11) as

$$\sum_{k=0}^{k_{max}} P_k^{(1)} g(C^* - kV) = \sum_{k=0}^{k_{max}} P_k^{(0)} g(kV - C^*), \tag{12}$$

where k, the number of contacts with the boundary, goes from 0 to k_{max}, with k_{max} being the largest possible number of contacts (determined by the number of lattice sites available at the boundary). Using the Fermi-Dirac equation for the function $g(C^* - kV)$ one gets

$$\sum_{k=0}^{k_{max}} \frac{P_k^{(1)} - P_k^{(0)} e^{\beta(C^* - kV)}}{1 + e^{\beta(C^* - kV)}} = 0. \tag{13}$$

Equation (13) is a nonlinear equation with one unknown, namely, C^*, which can be obtained once $P_k^{(0)}$ and $P_k^{(1)}$ are determined using simulations. From equation (9) it then follows that $\beta\Delta\mathcal{F} = \beta C^*$.

A special case that can be derived from equation (13) arises in the limit of $V \to \infty$. In this case, the polymer segments are excluded from the layer next to the moving object, *i.e.*, $P_0^{(1)} = 1$ and $P_k^{(1)} = 0$ and $e^{\beta(C^* - kV)} = 0$ for any $k \geq 1$. Equation (13) therefore reduces to

$$\frac{1 - P_0^{(0)} e^{\beta C^*}}{1 + e^{\beta C^*}} = 0,$$

which implies that

$$\beta C^* = \beta\Delta\mathcal{F} = -\ln P_0^{(0)}. \tag{14}$$

As already noted by Dickman [3], equation (14) is well-known and shows that if the probability of zero contacts at the boundary of the hard-body is known, one can get the change in free energy as the solid object is moved from $z = H$ to $z = H - 1$. Although very simple, this equation is not useful for cases where the density of the segments is high (*i.e.*, for high compressions) since the probability of zero contacts is very small and, therefore, hard to determine accurately. It is in such cases where the introduction of a *finite* repulsive potential at the boundary of the hard-body is desired. In doing so, one generates what can be thought of as *three* different systems: system 0 with $V = 0$, system 1 with $V = V_1$ and system 2 with $V = \infty$. It then follows that

$$\Delta\mathcal{F}_{0\to 2} = \Delta\mathcal{F}_{0\to 1} + \Delta\mathcal{F}_{1\to 2} \tag{15}$$

where $\Delta\mathcal{F}_{0\to 1}$ is obtained from equation (13) and $\Delta\mathcal{F}_{1\to 2}$ from equation (14) with $P_0^{(1)}$ in place of $P_0^{(0)}$. The major improvement of this scheme over previous methods is that it requires no extrapolations and less number of simulations.

In the procedure described above, the choice of the intermediate potential V_1 effective at the boundary of the moving object is arbitrary. According to Bennet [5], the statistical error in $\Delta\mathcal{F}$ depends on the extent of overlap

[1] For instance, in the two cases discussed in Section 4, the moving boundary is the bottom surface of an AFM tip.

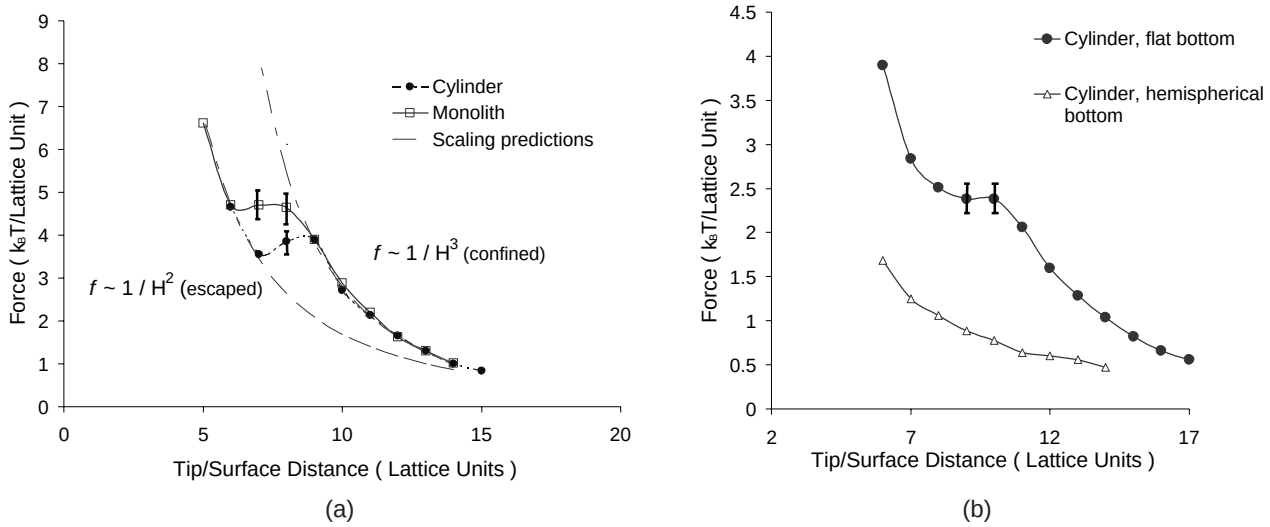

Fig. 1. Force due to compression and conformational transition in the case of a single, end-grafted chain in a theta solvent. The polymer chain is 100 segment long (*i.e.*, $N = 100$). The error bars in the force provide a measure of the fluctuations. (a) Shows the results for a flat-bottom cylindrical tip of radius $R_t = 60$ lattice units and for a square monolith with side $L_t = 120$. (b) Shows the results for cylindrical tips of radius $R_t = 50$ with flat and hemispherical bottoms. The forces are in units of k_BT/lattice unit, where k_B is the Boltzmann constant and T is the absolute temperature. (See, also, Jimenez and Rajagopalan [1].)

of the configurational spaces sampled in the two systems. Therefore, the idea is to choose a magnitude of V_1 such that the resulting distribution of contacts overlaps with the corresponding distribution obtained for $V = 0$ while, at the same time, guaranteeing that the probability of having zero contacts (when $V = V_1$) is obtained with good accuracy. For very dense systems it may be necessary to introduce one or more additional intermediate steps with repulsive potentials V_2, V_3, *etc.*, and decompose the total change in the Helmholtz potential into the appropriate number of contributions. The need for additional steps, however, has to be tested for each particular case. For example, we have tested the method using different values for V_1 and with a number of intermediate steps. The results show that, for our case, no additional steps were necessary and that the largest contribution to the error in $\Delta\mathcal{F}$ arises from the estimation of $\Delta\mathcal{F}_{1\to 2}$ from equation (14)[2], *i.e.*, propagation of the error from $P_0^{(1)}$.

4 Illustrative applications

In this section we illustrate the use of this method in two different problems, namely, the interaction of an AFM tip and a single end-grafted chain and the interaction of an AFM tip and a polymer *brush*.

[2] The error in $\Delta\mathcal{F}_{0\to 1}$ depends on the extent of overlap of the configurational spaces sampled from systems 0 and 1 and is inversely proportional to the number of (statistically independent) samples drawn from the simulations [5]. In our case, the error in $\Delta\mathcal{F}_{1\to 2}$ dominates even when only the tails of the contact distributions overlap.

4.1 Single end-grafted chain under compression

The first example we consider is the interaction between the tip of an atomic force microscope and an end-grafted polymer chain. Although primarily of theoretical interest, this situation serves as a convenient example for studying the force of compression, the accompanying conformational changes and the usefulness of scaling arguments. A number of issues influence the force measured and the conformations available to the chain in this case; these include, for example, the solvent quality and the shape and alignment of the tip (relative to the grafting point). Scaling theories can be developed in the simpler cases (*e.g.*, theta conditions and flat-bottom cylindrical tips) but cannot be extended to more complicated ones. The simulation method proposed in this paper offers a means to study the latter cases. Here, we illustrate the use of the method for some cases for which scaling theories are available [7,8] as well as for a few others that do not permit theoretical predictions.

Consider a polymer chain with N monomers end-grafted to a surface. The chain enters a metastable state as it is compressed by the flat bottom of a cylinder of radius R_t and will undergo a conformational transition from a "confined" state to an "escaped" state as the distance H between the bottom of the cylinder and the surface is decreased. Scaling laws can be developed for the Helmholtz potential $\mathcal{F}$ and the force of compression f in this case; for example, for theta conditions, Guffond *et al.* [8] have shown that

$$\mathcal{F}_{confined} = c_1 \frac{Na^2}{H^2}; \qquad f_{confined} = 2c_1 \frac{Na^2}{H^3} \tag{16}$$

and

$$\mathcal{F}_{escaped} = 2c_2\frac{R_t}{H}; \qquad f_{escaped} = 2c_2\frac{R_t}{H^2}, \qquad (17)$$

where a is the monomer size and c_1 and c_2 are proportionality constants. The transition from the confined to the escaped state occurs at a distance H^*, the crossover point between the free energies of the two states,

$$H^* = \frac{c_1}{c_2}\,\frac{Na^2}{2R_t}, \qquad (18)$$

which, according to equations (16, 17), corresponds to a sudden change in the force profile. In reality, however, the transition will be less drastic as the conformation of the chain fluctuates between the two states. One would expect the extent of the "noise" in the force in the transition region to depend on the free energy barrier between the two states and the temperature (or the quality) of the solvent. Scaling relations cannot, of course, predict this noise, but simulations can.

The contact-distribution method described in the last section offers a computational scheme to test such scaling relations and to examine the details of the transition region as we have illustrated in a preliminary communication elsewhere [1]. Figure 1 presents such an application of the contact-distribution method for three types of compressing objects. The results for a flat-bottom monolith and a flat-bottom cylinder in Figure 1a reveal that the scaling relations developed for the cylindrical tip are also valid for monoliths with the same linear dimension, although, as one would expect qualitatively, the onset of escape for the monolith occurs at a smaller value of H. In addition, the simulations give details on the transition region, which is dominated by thermal noise[3]. The latter information is accessible only through simulations and cannot be deduced from scaling arguments. Figure 1b also illustrates another extension that is not accessible through scaling arguments, *i.e.*, compression with a hemispherical tip. The force profile for this case differs markedly from the result for compression using a flat-bottom tip, both in magnitude and in the functional form.

Figure 2 illustrates the influence of another important property, namely, the quality of the solvent (or, the temperature), on the force and escape behavior. It can be seen from Figure 2 that there is a critical temperature beyond which thermal fluctuations blur the characterization of the states as confined or escaped. It is also evident from this figure that the functional form of the force for large H for good solvents differs noticeably from what is expected for theta solvents. (Scaling arguments for good solvents suggest that $f \sim H^{-8/3}$ [7].) In contrast, at small H, the forces for both cases follow the same form since the differentiation between good solvent and theta solvent loses its meaning at high compression.

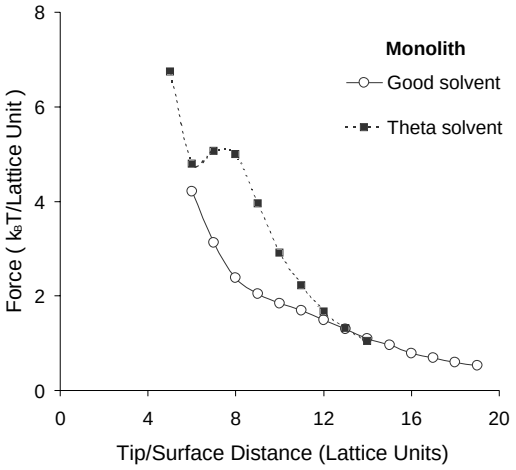

Fig. 2. Forces in the case of a single, end-grafted chain (number of segments $N = 100$) compressed by a monolith with a square cross-section ($L_t = 120$) in good and theta solvents.

Our objective here is to merely demonstrate the types of information accessible through the contact-distribution method. Some additional details on these issues may be found in reference [1].

4.2 Compression of a polymer brush

In this section we consider an extension of the case discussed above, namely, the force of compression of a polymer *brush* in a theta solvent.

The lattice simulations used for this purpose employ the three-dimensional bond-fluctuation model already described in the literature [9–11]. A lattice size of $40 \times 40 \times 100$ is used with impenetrable walls at $z = 0$ and $z = 100$ and with periodic boundary conditions in the x- and y-directions. The simulations consider m chains with N segments each, and each chain is end-grafted to the lower wall in a periodic array. The segments interact with each other through a square-well potential [11] with an interaction parameter given by $\chi/k_BT = -0.53$. This interaction gives rise to a behavior characteristic of theta conditions [11]. The shape and the size of the tip used to obtain the results are listed in Table 1. For each set of parameters, several simulations are run for different values of H (with at least one run for each H). In each case, the system is first equilibrated and then sampled over $1{-}3\times10^7$ Monte-Carlo steps to obtain the probability of the chain having k contacts with the tip. Equations (13, 14) are then used to estimate the change in the Helmholtz potential.

To the best of our knowledge, only one previous attempt has been made on the simulation of the interaction between an AFM tip and a polymer brush. This work, by Murat and Grest [12], uses molecular dynamics

[3] As noted previously, the noise observed in the force obtained from the simulations arises from the propagation of errors in the calculation of $\Delta\mathcal{F}_{1\to2}$ from equation (14). It should be noted that, within the transition region, the fluctuations in $P_0^{(1)}$ cannot be reduced by increasing the number of samples drawn from the simulations.

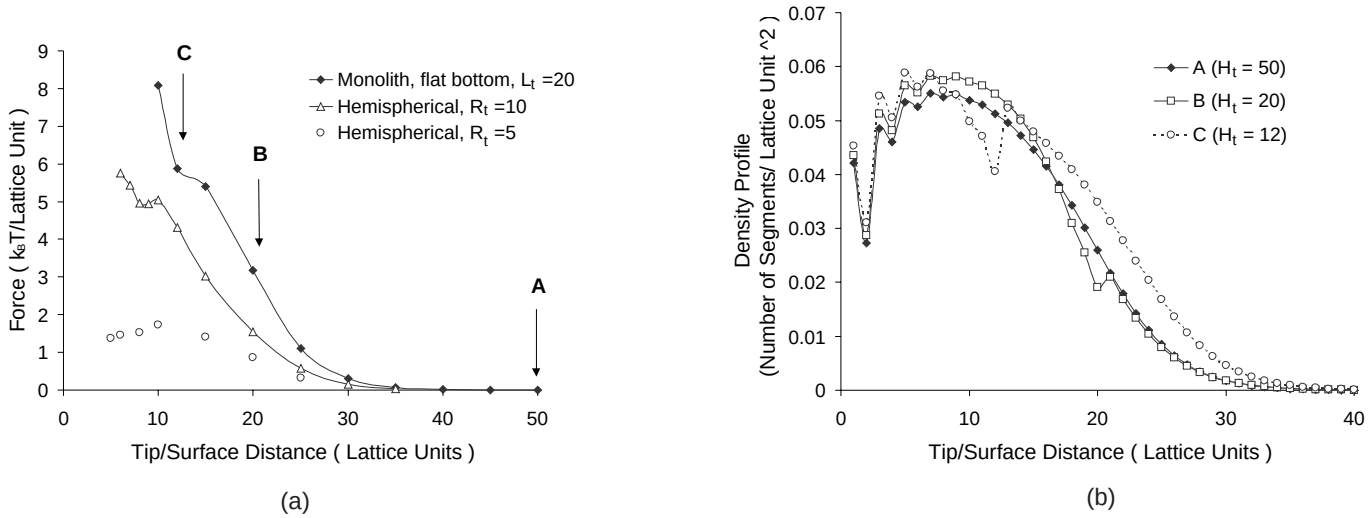

Fig. 3. (a) Force between an AFM tip and a polymer brush in a theta solvent. The simulation parameters are specified in Table 1. The radius of gyration, R_{gxy}, in the x-y plane under these conditions is 5.6 lattice units. (b) Segment density profiles of the brush for three different positions of the AFM tip as indicated in Figure (a) for the monolith. The parameters used correspond to case I in Table 1. Densities are in number of segments per unit area parallel to the surface.

Table 1. Parameters used for Figure 3.

Case	Tip Size	Tip Shape
I	$L_t = 20$	Monolith, Flat Bottom
II	$R_t = 10$	Cylinder, Hemispherical Bottom
III	$R_t = 5$	Cylinder, Hemispherical Bottom

Note: the grafting density is held constant at 0.1. The number of chains, m, is 40, each with 40 segments.

simulations to obtain the effect of the shape and size of the tip on the force profile under good-solvent conditions. The results show that the polymer chains splay-out upon compression, thereby giving rise to a deviation of the force from theoretical predictions based on the assumption that the chains cannot escape from under the tip in the brush regime [13].

In contrast to the work of Murat and Grest [12], the present work focuses on the AFM tip/polymer brush interactions under *theta* conditions. We have selected the theta condition here in view of the interesting conformational transition shown in Figure 1 for single chains. It is, therefore, interesting to examine if such a transition exists in the case of a polymer brush. (The calculations of Murat and Grest [12] do not indicate such a transition at good-solvent conditions. However, our results for the *mushroom* reported in the previous section suggest that the demarcation of the states as confined or escaped and, therefore, the "transition region" lose their meanings in good solvents because of thermal fluctuations.)

Figures 3a and 3b present some results for the case of a brush in theta solvents and illustrate the qualitatively different behaviors that can be expected depending on the magnitude of $R_t^* = (R_t/R_{gxy})$, the relative size of the tip R_t with respect to the radius of gyration R_{gxy} of the chain in the x- and y-directions. (The magnitude of R_{gxy} for the examples shown is roughly 5.6 lattice units.)

– For $R_t^* \leq 1$, one cannot speak of "compression" of the chains since the tip penetrates the brush easily (and, as a result, the force is essentially constant), whereas for $R_t^* > 1$ conformational rearrangements in the chains can be seen for the conditions illustrated in the figure. This effect manifests itself in the force profile through a "transition" region, which is discussed below in more detail.
– The conformational rearrangements can also be observed from the segment density profiles shown in Figure 3b (for a monolith) for three different positions of the AFM tip. These positions are marked by Points A, B and C in Figure 3a and correspond to $H_t = 50, 20$ and 12, respectively. Curve A in Figure 3b illustrates the density profile for an *unperturbed* brush (*i.e.*, the tip is quite far from the brush). The segment density profile corresponding to position B (curve B in Fig. 3b) shows that the chains under the tip are in a "confined" state, indicated by the increased density for $H \lesssim 16$. (The decrease in density for $16 \lesssim H \leq H_t = 20$ is the result of packing restrictions.) For $H > 20$, the density is essentially the same as that for a free brush. The situation in curve B thus corresponds essentially to pure compression of the chains beneath the tip. In contrast, a significant level of "escape" can be seen for curve C ($H_t = 12$), as evident from the increase in the density for $H > 12$. The densities reported are computed over an area four times the cross-sectional area of the tip for calculations beneath the tip ($H < H_t$) and over an area three times the tip area for $H > H_t$ (*i.e.*, the area occupied by the tip is not available for the chains). The above results are meant to merely illustrate the

conformational changes arising from the compression. In general, for detailed quantitative analyses, the area used for calculating the densities must be small enough to reflect the density changes in the neighborhood of the tip accurately. In addition, the size of the simulation box must be large enough to avoid the effect of the periodic boundary condition on the calculations.

The implications of the effects illustrated above to the interpretation of the forces measured using an AFM are discussed elsewhere [1] in the context of the compression of a single chain.

In the two cases presented above, the AFM tip is considered as a semi-infinite object, that is, the object is not fully contained within the simulation box. The contact-distribution method can, however, be applied to situations involving finite-sized objects, but the estimation of the change in free energy requires some additional steps. The additional steps are required since the introduction of a repulsive potential to a portion of a finite object (such as a spherical particle) results in a *distortion*, rather than a displacement, of the particle. If one denotes the distorted state as system 3 and the original and the new positions of the objects as systems 1 and 2, respectively, the required result, $\Delta\mathcal{F}_{1\to 2}$, is then obtained from

$$\Delta\mathcal{F}_{1\to 2} = \Delta\mathcal{F}_{1\to 3} - \Delta\mathcal{F}_{2\to 3}. \tag{19}$$

We shall consider this in a forthcoming publication.

5 Concluding remarks

We have introduced a new method for determining the Helmholtz potential differences and forces in polymer and colloid mixtures from lattice Monte-Carlo simulations. The method has been used to obtain the force due to the compression of an end-grafted polymer chain with an AFM tip and due to the compression of a polymer brush. The results illustrate how the method can be used to test or extend scaling theories and to examine conformational transitions. The method introduced here can be easily extended to systems with physisorbed chains and for interactions between finite objects in polymer solutions.

We would like to thank the National Science Foundation (CTS-986097), the Engineering Research Center (ERC) for Particle Science and Technology at the University of Florida (NSF EEC-9402989) and the Industrial Partners of the ERC for partial support of the work presented here.

References

1. J. Jimenez, R. Rajagopalan, Langmuir **14**, 2598 (1998).
2. R. Dickman, D. Hong, J. Chem. Phys. **95**, 4650 (1991).
3. H.P. Deutsch, R. Dickman, J Chem. Phys. **93**, 8983 (1990).
4. R. Dickman, P.E. Anderson, J. Chem. Phys. **99**, 3112 (1993).
5. C. Bennet, J. Comput. Phys. **22**, 245 (1976).
6. D. Frenkel, B. Smit, *Understanding Molecular Simulation* (Academic Press, New York, NY, 1996).
7. G. Subramanian, D.R.M. Williams, P.A. Pincus, Europhys. Lett. **29**, 285 (1995).
8. M.C. Guffond, D.R.M. Williams, E.M. Sevick, Langmuir **13**, 5691 (1997).
9. I. Carmesin, K. Kremer, Macromol. **21**, 2819 (1988).
10. P.Y. Lai, K. Binder, J. Chem. Phys. **95**, 9288 (1991).
11. P.Y. Lai, K. Binder, J. Chem. Phys. **97**, 586 (1992).
12. M. Murat, G. Grest, Macromol. **29**, 8282 (1996).
13. G. Subramanian, D.R.M. Williams, P.A. Pincus, Macromol. **29**, 4045 (1996).